Anisotropic in-plane strain and transport in epitaxial $Nd_{0.2}Sr_{0.8}MnO_3$ thin films

K. P. Neupane,[1,a)] J. J. Neumeier,[2] and J. L. Cohn[1,b)]
[1]*Department of Physics, University of Miami, Coral Gables, Florida 33124, USA*
[2]*Department of Physics, Montana State University, Bozeman, Montana 59717, USA*

(Received 2 October 2009; accepted 26 October 2009; published online 18 December 2009)

The structure, morphology, and electrical properties of epitaxial *a*-axis-oriented thin films of $Nd_{0.2}Sr_{0.8}MnO_3$ are reported for thicknesses of 10 nm$\leq t \leq$150 nm. Films were grown with both tensile and compressive strain on various substrates. It is found that the elongated crystallographic *c*-axes of the films remain fully strained to the substrates for all thicknesses in both strain states. Relaxation of the *a* and *b* axes is observed for $t \gtrsim 65$ nm, with films grown under tensile strain developing uniaxial crack arrays (running along the *c* axis) due to a highly anisotropic thermal expansion. For the latter films, the room-temperature in-plane electrical resistivity anisotropy, ρ_b/ρ_c, increases approximately exponentially with increasing film thickness to values of ~1000 in the thickest films studied. Films under tension have their Néel temperatures enhanced by ≈25 K independent of thickness, consistent with an enhancement in ferromagnetic exchange along their expanded *c* axes. © *2009 American Institute of Physics*. [doi:10.1063/1.3269698]

I. INTRODUCTION

Using strain in thin films to achieve expanded or contracted lattices of novel materials has proven fruitful in producing new phases or functionalities for known bulk compounds. An interesting avenue of investigation is the growth of anisotropically strained films of perovskite oxides. The heavily hole-doped perovskite manganites that order in the C-type antiferromagnetic (AF) arrangement,[1,2] e.g., $Nd_{1-x}Sr_xMnO_3$ with $0.75 \leq x \leq 0.9$, are of interest in this regard. Bulk single crystals of compounds with $x \gtrsim 0.8$ have proven difficult to grow. The C-type AF state consists of a one-dimensional ordering of $d_{3z^2-r^2}$ orbitals of the Mn^{3+} sites oriented along the elongated *c* axis of the tetragonal structure, facilitating ferromagnetic (FM) coupling of Mn^{3+} and Mn^{4+} spins along *c* and an AF spin alignment along the *a* axes.[3] *a*-axis-oriented films under anisotropic strain should allow for the manipulation of the FM double-exchange and AF superexchange interactions responsible for this ordering.[4,5] They should make accessible the study of intrinsic electrical anisotropy, a motivation for which is the large static dielectric constant ($\epsilon \sim 100$) observed[6] in polycrystalline $Ca_{0.2}La_{0.8}MnO_3$, and hypothesized to arise from an enhanced polarizability along the one-dimensional *c*-axis in the AF phase.

Relevant to the successful growth of *a*-axis films of these compounds are thermal expansion coefficients along the *a* and *c* axes that are opposite in sign in a broad temperature range from the cubic-tetragonal transition to well below room temperature (a consequence of the orbital ordering).[2] This differential thermal expansion induces highly anisotropic and temperature-dependent in-plane strain. We find that thicker films under anisotropic tensile strain within the substrate plane develop uniaxial crack arrays with regular crack spacing on the order of 1 μm. These crack arrays yield in-plane electrical resistivities that are highly anisotropic with an anisotropy ratio that varies approximately exponentially with film thickness, reaching values of $\gtrsim 10^3$. The Néel temperatures of films under tensile strain are enhanced by 25 K, independent of thickness, over those of the bulk target and compressively strained films, consistent with an increased stability of the orbital and spin order that is controlled principally by the *c*-axis length.

II. EXPERIMENT

The polycrystalline target of nominal composition $Nd_{0.2}Sr_{0.8}MnO_3$ (NSMO) was prepared by conventional solid state reaction as described elsewhere.[7] Thin films were grown by pulsed laser deposition on pseudocubic (110)-oriented $(LaAlO_3)_{0.3}$-$(Sr_2AlTaO_6)_{0.7}$ (LSAT) (a =0.3868 nm) and $LaAlO_3$ (LAO) (a=0.379 nm), and orthorhombic (100)-oriented $NdGaO_3$ (NGO) (a=0.543 nm, b =0.550 nm, c=0.771 nm) substrates. An excimer laser (KrF: λ=248 nm) with a frequency of 10 Hz and an energy density of ~1–2 J/cm^2 were employed. The substrate temperature was 750 °C and partial oxygen pressure 260 mTorr. Following deposition, films were cooled in ~760 Torr O_2 at 1 °C/min to 500 °C and held for 1 h before cooling to room temperature. The crystallographic orientation, film thickness (t), and lattice constants were evaluated using a Philips X'Pert x-ray diffractometer (Cu Kα radiation). Surface morphology was studied with scanning electron microscopy (SEM). Four-probe, in-plane dc resistivity (with silver epoxy contacts) was measured on specimens with typical dimensions $6 \times 1.3 \times t$ mm^3. The room-temperature thermopower (TEP) was measured for all specimens with a steady-state method using gold leads and a chromel-constantan thermocouple.

[a)]Present address: 201-1650 Pembina Highway, Winnipeg, Manitoba R3T2G3, Canada.
[b)]Electronic mail: cohn@physics.miami.edu.

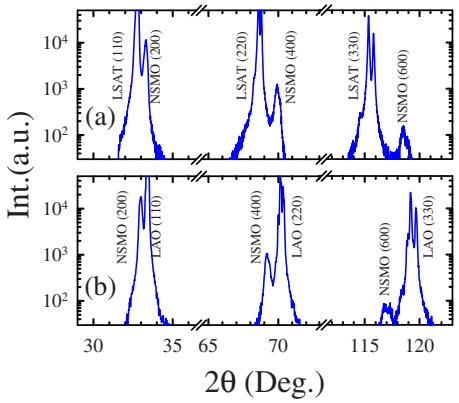

FIG. 1. (Color online) $2\theta/\omega$ scans of NSMO films: (a) 130 nm on (110) LSAT, (b) 150 nm on (110) LAO.

The target lattice constants, $a=0.5390(5)$ nm, $c=0.766(1)$ nm are in reasonable agreement with those reported by Kajimoto *et al.*[1] for crushed, melt-grown crystals at lower doping. The value of the Néel temperature, $T_N \simeq 242$ K was inferred from the peak in $d \log \rho / d(1/T)$ (further discussed below).

III. RESULTS AND DISCUSSION

A. Lattice constants and morphology

All of the films are orthorhombic with their longer c axes in the film plane. Taking the a axis in the growth direction, the (100) orientation of the films is indicated in x-ray diffraction 2θ-ω scans, shown for 130-nm-thick films grown on LSAT (110) and LAO (110) in Figs. 1(a) and 1(b), respectively, by the presence of only $(2h,0,0)$ film reflections near the $(h,h,0)$ substrate reflections. Phi scans of asymmetric film and substrate reflections, shown in Fig. 2 for the 130-nm-film grown on LSAT, confirm the cube-on-cube orientation with NSMO [010]‖LSAT $[1\bar{1}0]$ and NSMO [001]‖LSAT [001]; the same orientation relationship was found for films grown on LAO. X-ray results for the films on NGO indicate NSMO [010]‖NGO [010] and NSMO [001]‖NGO [001].

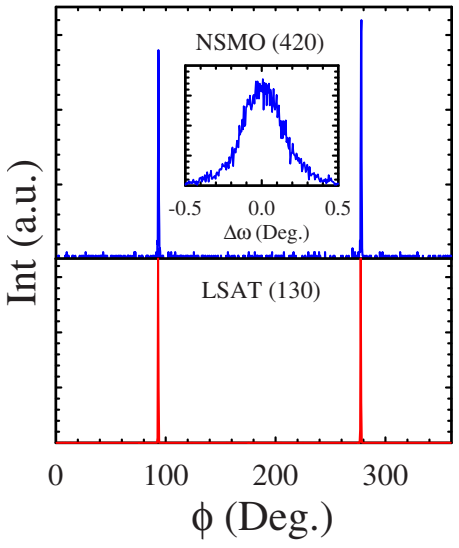

FIG. 2. (Color online) Azimuthal (ϕ) scans of the (420) film (upper panel) and (130) substrate (lower panel) reflections for the 130-nm-film grown on (110) LSAT, confirming epitaxial growth. The inset shows the rocking-curve width for the film reflection.

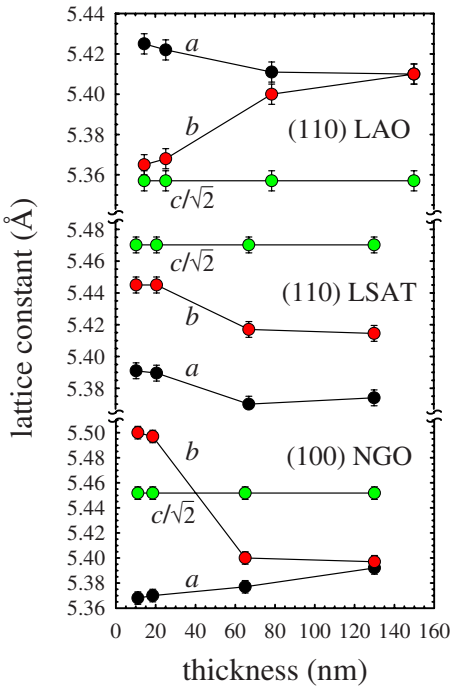

FIG. 3. (Color online) Lattice constants vs thickness for NSMO films on three substrates.

The lattice constants for all films were determined from reciprocal space maps in the vicinity of the film (600), (440), (620), and (404) reflections, with nearby substrate reflections serving as internal references. The corresponding NGO reflections have the same indices as the films. For (110)-oriented LAO and LSAT the corresponding substrate reflections are (330), (400), (420), and (222), respectively. Figure 3 shows lattice constants as a function of film thickness for films on the three substrates. For all substrates and thicknesses, the film c-axes are fully strained to those of the substrate. The a and b axis lengths are clearly relaxed in response to the compressive (LAO) and tensile (LSAT, NGO) in-plane strain along the film [010] directions, with the most substantial effect occurring for NGO.

For LAO films the result is an expansion along [010] and contraction along the film normal ([100]), whereas for NGO films the b-axes contract and the a-axes expand. For both substrates the thickest film is tetragonal. The films on LSAT exhibit more modest contractions along both [010] and [100] with increasing thickness, maintaining orthorhombicity. In spite of these differences in behavior for the NGO and LSAT films under tensile strain, their unit cell volumes (Fig. 4) show very similar decreases with increasing thickness.

Scanning electron micrographs (Fig. 5) demonstrate that the relaxation of tensile strain along [010] for the films on NGO and LSAT is accommodated by the formation of unidirectional crack arrays running along the film [001] direction. The spacing of these cracks, determined from analyses of larger-area images from films on each of the substrates, approximately describes a log-normal distribution [shown in Fig. 5(c) for the 65-nm NGO film], with median values of

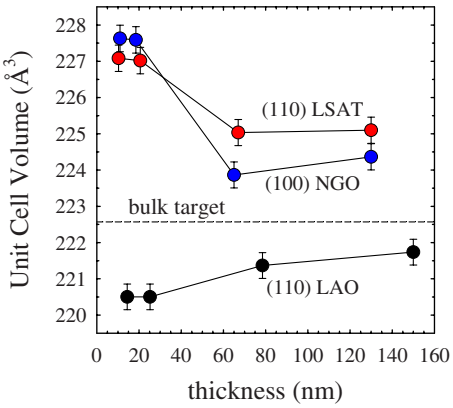

FIG. 4. (Color online) Unit cell volume vs thickness for NSMO films on three substrates.

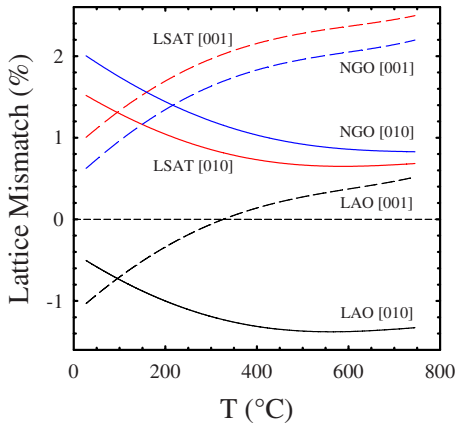

FIG. 6. (Color online) Lattice mismatch vs temperature for the three substrates along the film [010] and [001] directions. Positive values correspond to a substrate lattice constant larger than that of the film.

$\sim 1-2$ μm and $\sim 3-4$ μm for LSAT and NGO films, respectively. These distributions did not change appreciably with thickness for either substrate. The width of the cracks themselves varies within a given film [particularly evident in Fig. 5(b) for the NGO film], and the mean crack width is greater in the thicker films. Though transverse-sectional microscopy was not pursued, as we discuss further below the transport data implies that the cracks do not penetrate through to the substrate.

Similar crack arrays were observed previously[8] for [110]-oriented $YBa_2Cu_3O_{7-\delta}$ and $PrBa_2Cu_3O_{7-\delta}$ films grown on [110] $SrTiO_3$, where they were attributed to anisotropic thermal expansion mismatch between substrate and film upon cooling from the growth temperature. The same mechanism appears applicable to the present oxide film-substrate systems since, as noted above, NSMO has thermal expansion coefficients of opposite sign: positive along [010] and negative along [001].[2] The lattice mismatch, $(a_{sub}-a_{NSMO})/a_{sub}$ (a_{sub} and a_{NSMO} are the substrate and bulk target lattice constants, respectively) is shown as a function of temperature in Fig. 6 along the [010] and [001] film directions for each of the three substrates. These curves were computed using published thermal expansion data for the substrates.[9,10] The target lattice constants were measured up to 200 °C and their temperature dependencies found to match well those of Tobe *et al.*[2] measured over a broader temperature range for compounds with a slightly different stoichiometry; the target data were then extended to higher temperature using the suitably scaled expansion data.

At the growth temperature (750 °C) the tensile mismatch for LSAT and NGO is greatest along the film [001] direction. Upon cooling, the mismatch along [001] decreases since the *c*-axis expands, while that along [010] increases. For the films on NGO the [010] mismatch approaches 2% at room temperature, the same amount by which the *b*-axis lattice parameter decreases abruptly with increasing thickness. Although the calculated compressive mismatch along [010] for films on LAO is only 0.5% at room temperature, the compressed lattice is only stable at low thicknesses. Evidently there is a comparable critical thickness for NSMO above which both compressed and expanded lattices are relaxed.

In spite of the linear crack arrays that develop in the thicker films under tensile strain, all of the films remain smooth as indicated by well-defined Kiessig oscillations seen in x-ray reflectivity measurements over an extended angular range (Fig. 7). Reflectivity simulations[11] imply a film surface

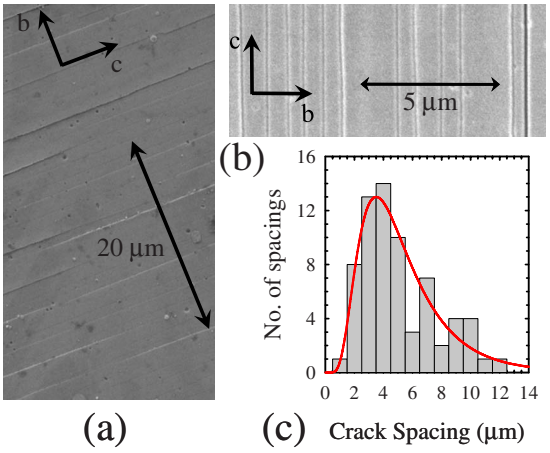

FIG. 5. (Color online) SEM images of (a) 67-nm-film on (110) LSAT, (b) 130-nm-film on (100) NGO, and (c) distribution of crack spacings for the NGO film. The solid curve is a log-normal distribution with median =3.5 μm and geometric standard deviation=1.26 μm.

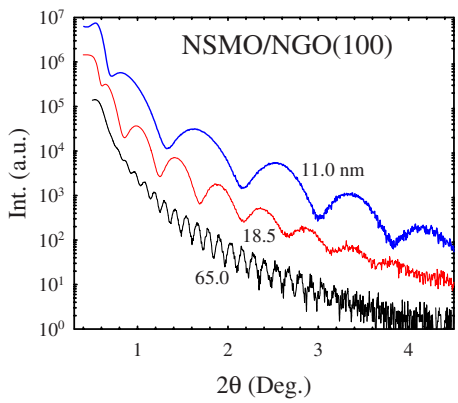

FIG. 7. (Color online) (a) X -ray reflectivity for three films deposited on (100) NGO. Curves are offset vertically for clarty.

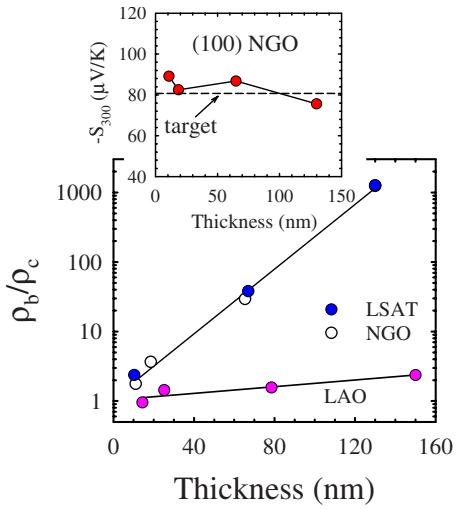

FIG. 8. (Color online) Room-temperature in-plane resistivity ratio, ρ_b/ρ_c, vs thickness for films grown on three substrates.

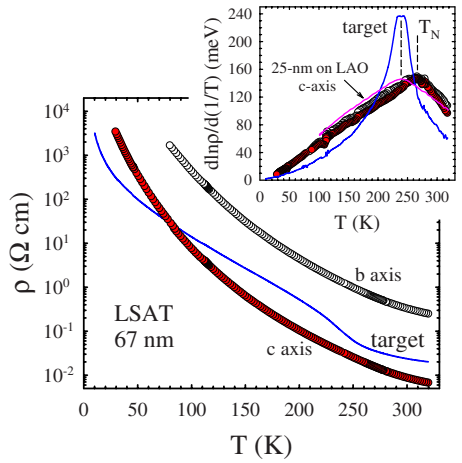

FIG. 9. (Color online) $\rho(T)$ along the b and c axes of the 67-nm-film grown on (110) LSAT. The solid curve represents the resistivity of the bulk, polycrystalline target. The inset shows $d \ln \rho(T)/d(1/T)$ vs T for the same specimens and for the 25-nm-LAO film along the c axis.

roughness with variance $\sigma \sim 0.4$ nm for the thinnest films, comparable to the perovskite unit cell dimension, with a modest increase for thicker films.

B. Transport Properties

The dc electrical resistivity was measured for each film along the [010] and [001] directions as a function of temperature for $T \leq 325$ K. Film resistances exceeding 1 GΩ prevented measurements below ~50 K. The room-temperature resistivity anisotropy, ρ_b/ρ_c, is found to increase approximately exponentially with increasing film thickness for the LSAT and NGO films (Fig. 8), reflecting principally an increase along [010] due to cracking. For the thickest films $\rho_b/\rho_c \simeq 1000$. The corresponding ratio for the LAO films also increases with thickness, reaching $\rho_b/\rho_c \simeq 2.4$ for the 150-nm-film. As this thickest film is tetragonal with unit cell volume and T_N closest to the bulk target (Fig. 3), we take the latter value to be representative of the intrinsic anisotropy of the NSMO compound.

To investigate the possibility that variations in oxygen content with thickness might contribute to the changes in resistivity, the room-temperature TEP was measured for all films. The TEP is a sensitive measure of Mn valence that is largely independent of cation in this region of the manganite phase diagram.[12,13] The value measured for the target was −80 μV/K. The TEPs for the films did not vary by more than ~10% for all thicknesses, typically falling in the range −(80–100) μV/K, as shown for the NGO films in the inset of Fig. 8. Thus significant and systematic variations in the oxygen content of the films with thickness are ruled out.

Figure 9 shows the T dependence of the in-plane resistivities for the 67-nm-film grown on (110) LSAT along with that of the target. Interestingly, in spite of the substantial resistive anisotropy ($\rho_b/\rho_c \simeq 35$ for this film), the T dependencies are essentially identical along the [010] and [001] directions (inset, Fig. 9). This implies that the cracks do not penetrate into the substrate, since a stronger temperature dependence along [010] would be expected associated with thermally activated tunnel conduction as observed in other cracked manganite films.[14]

The AF transition temperatures, T_N, determined from maxima in $d \ln \rho(T)/d(1/T)$ versus T (inset, Fig. 9), are 265 ± 3 K for LSAT and NGO films, and $T_N = 240 \pm 3$ K, the same as the bulk target, for films grown on LAO. In G-type AFs such as $Ca_{1-y}Sr_yMnO_3$, expansion of the lattice due to Sr substitution[15] enhances AF superexchange interactions (and T_N) due to an increase in the Mn–O–Mn bond angle. Stability of the C-type AF ordered state is increased by structural modifications tending to isolate the FM one-dimensional chains.[5] In the present films it seems likely that the significant enhancement in T_N for films with expanded unit cells is principally due to the expansion along [001]. Though enhanced superexchange, e.g., due to an increase in the Mn–O–Mn bond angles along [100] and [010] is possible, the observation that T_N for these films is independent of thickness, in spite of the very different b-axis lengths due to cracking in the thicker films, argues against its prominent role in determining the increase in T_N. More likely is that the expansion along [001] actually enhances the double-exchange coupling along [001] in this compound, thereby increasing the stability of the orbital and C-type Néel ordering.[5] We note that the c-axis length in the bulk target is ≃1.2% smaller than that of a $x=0.75$ compound[1] with $T_N \simeq 300$ K. Thus the observed increase in T_N for the films under tension is consistent with existing data on the structure and phase behavior in this regime of composition, where T_N is plausibly controlled principally by the c-axis length.

IV. CONCLUSION

Epitaxial a-axis-oriented films of $Nd_{0.2}Sr_{0.8}MnO_3$ have been grown under both compressive and tensile strain. The intrinsic resistivity anisotropy of the material, inferred from transport measurements on a 150-nm-thick, compressively strained film, is $\rho_b/\rho_c = 2.4$. Uniaxial crack arrays oriented along the film [001] direction develop in films under tensile strain with thickness ≳65 nm due to anisotropic thermal ex-

pansion mismatch upon cooling from the growth temperature. Typical crack spacings are a few micrometers. The resistivity anisotropy measured for the cracked films exceeds 10^3. Identical temperature dependencies of the resistivity along and transverse to the cracks imply that not all penetrate through to the substrate, and thus the large anisotropy is attributed to a thin and meandering conduction path for transport along [010]. The increased Néel temperature for films under tensile strain, from 240 K for the bulk target to 265 K independent of thickness, suggests that enhanced FM exchange stabilizes the orbital and spin order of the C-type AF state, and that their stability in this region of the phase diagram is largely controlled by the *c*-axis length.

ACKNOWLEDGMENTS

We thank Mr. Alsayegh Husain for technical assistance with SEM scanning. This material is based on work supported by the National Science Foundation under Grant Nos. DMR-0072276 (Univ. Miami) and DMR-0504769 (Montana State Univ.), the Research Corporation (Univ. Miami), and the U.S. DOE Office of Basic Energy Sciences (Montana State Univ., Grant No. DE-FG-06ER46269).

[1]R. Kajimoto, H. Yoshizawa, H. Kawano, H. Kuwahara, Y. Tokura, K. Ohoyama, and M. Ohashi, Phys. Rev. B **60**, 9506 (1999).
[2]K. Tobe, T. Kimura, and Y. Tokura, Phys. Rev. B **67**, 140402(R) (2003); **69**, 014407 (2004).
[3]R. Kajimoto, H. Yoshizawa, R. Kawasaki, K. Noda, and H. Kuwahara, J. Phys. Soc. Jpn. **74**, 502 (2005).
[4]R. Maezono, S. Ishihara, and N. Nagaosa, Phys. Rev. B **57**, R13993 (1998); **58**, 11583 (1998).
[5]J. van den Brink and D. Khomskii, Phys. Rev. Lett. **82**, 1016 (1999); I. V. Solovyev and K. Terakura, Phys. Rev. B **63**, 174425 (2001).
[6]J. L. Cohn, M. Peterca, and J. J. Neumeier, Phys. Rev. B **70**, 214433 (2004).
[7]H. Terashita and J. J. Neumeier, Phys. Rev. B **71**, 134402 (2005).
[8]E. Olsson, A. Gupta, M. D. Thouless, A. Segmüller, and D. R. Clarke, Appl. Phys. Lett. **58**, 1682 (1991); M. D. Thouless, E. Olsson, and A. Gupta, Acta Metall. Mater. **40**, 1287 (1992).
[9]B. C. Chakoumakos, D. G. Schlom, M. Urbanik, and J. Luine, J. Appl. Phys. **83**, 1979 (1998).
[10]W. Marti, P. Fischer, F. Altorfer, H. J. Scheel, and M. Tadin, J. Phys.: Condens. Matter **6**, 127 (1994); A. Senyshyn, L. Vasylechko, M. Knapp, U. Bismayer, M. Berkowski, and A. Matkovskii, J. Alloys Compd. **382**, 84 (2004); O. Chaix-Pluchery, B. Chenevier, and J. J. Robles, Appl. Phys. Lett. **86**, 251911 (2005).
[11]W. Spirkl, J. Appl. Phys. **74**, 1776 (1993).
[12]J. Hejtmánek, Z. Jirák, M. Marysko, C. Martin, A. Maignan, M. Hervieu, and B. Raveau, Phys. Rev. B **60**, 14057 (1999).
[13]J. L. Cohn, C. Chiorescu, and J. J. Neumeier, Phys. Rev. B **72**, 024422 (2005).
[14]K. M. Satyalakshmi, B. Fisher, L. Patlagan, and G. Koren, Appl. Phys. Lett. **73**, 402 (1998).
[15]O. Chmaissem, B. Dabrowski, S. Kolesnik, J. Mais, D. E. Brown, R. Kruk, P. Prior, B. Pyles, and J. D. Jorgensen, Phys. Rev. B **64**, 134412 (2001).